

Supplement to Progressive Simulation for Cloth Quasistatics

JIAYI ERIS ZHANG, Adobe & Stanford University, USA

JÈRÈMIE DUMAS, Adobe, USA

YUN (RAYMOND) FEI, Adobe, USA

ALEC JACOBSON, Adobe & University of Toronto, Canada

DOUG L. JAMES, Stanford University, USA

DANNY M. KAUFMAN, Adobe, USA

CCS Concepts: • Computing methodologies → Physical simulation.

Additional Key Words and Phrases: Progressive Simulation, Multiresolution, Cloth Simulation, Contact Mechanics

ACM Reference Format:

Jiayi Eris Zhang, Jérémie Dumas, Yun (Raymond) Fei, Alec Jacobson, Doug L. James, and Danny M. Kaufman. 2022. Supplement to Progressive Simulation for Cloth Quasistatics. *ACM Trans. Graph.* 41, 6, Article 218 (December 2022), 4 pages. <https://doi.org/10.1145/3550454.3555510>

1 CONSISTENCY MEASURES FROM CURVATURE DIFFERENCES

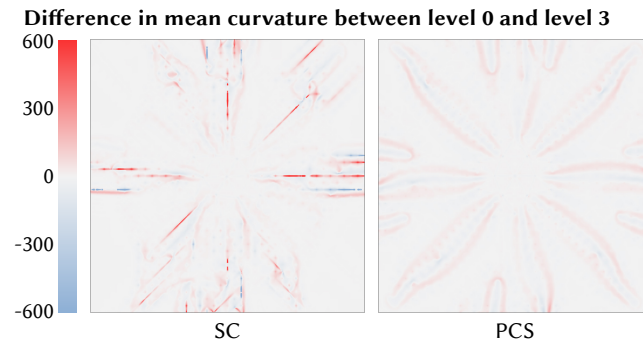


Fig. 1. We compare the pointwise difference in mean curvature for SC and PCS, on their common flat base-domain, for their respective final drapes of the cloth on sphere example from Figure 4 in the main paper. Here the SC method exhibits regions of large difference in curvature (correlating with inconsistent wrinkles).

Authors' addresses: Jiayi Eris Zhang, Adobe & Stanford University, USA, eriszh@stanford.edu; Jérémie Dumas, Adobe, USA, jedumas@adobe.com; Yun (Raymond) Fei, Adobe, USA, yfei@adobe.com; Alec Jacobson, Adobe & University of Toronto, Canada, jacobson@cs.toronto.edu; Doug L. James, Stanford University, USA, djames@cs.stanford.edu; Danny M. Kaufman, Adobe, USA, dannykaufman@gmail.com.

Permission to make digital or hard copies of all or part of this work for personal or classroom use is granted without fee provided that copies are not made or distributed for profit or commercial advantage and that copies bear this notice and the full citation on the first page. Copyrights for components of this work owned by others than ACM must be honored. Abstracting with credit is permitted. To copy otherwise, or republish, to post on servers or to redistribute to lists, requires prior specific permission and/or a fee. Request permissions from permissions@acm.org.

© 2022 Association for Computing Machinery.

0730-0301/2022/12-ART218 \$15.00

<https://doi.org/10.1145/3550454.3555510>

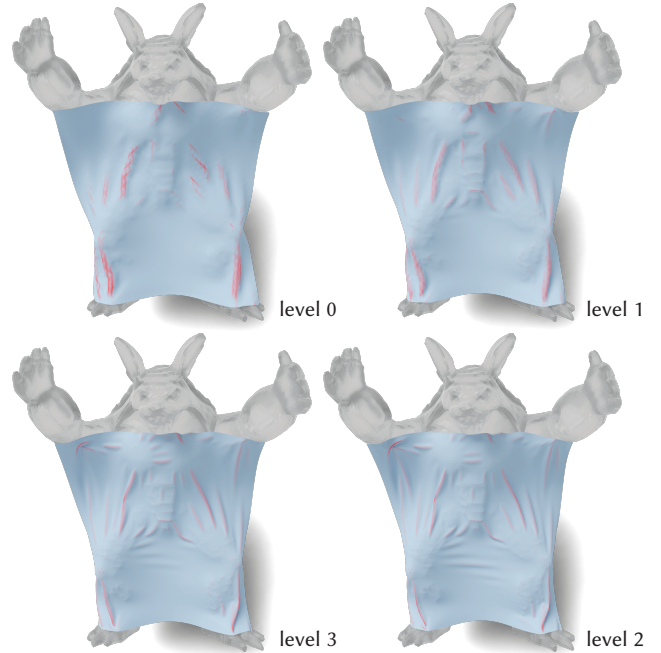


Fig. 2. Fold consistency across levels. We visualize thresholded principal curvature to highlight how folds and wrinkles remain consistent across levels for this PCS drape.

We are interested in quantitatively assessing the consistency between different resolution levels of cloth simulation. Because all levels are surfaces over a common parametrization of a domain Ω , one family of measures is the difference of curvature integrated over this parametric domain. For example, we may compute the total integral of squared difference in mean curvature as

$$d_H = \int_{\Omega} \|H_c - H_f\|^2 dA,$$

where H_c and H_f are pointwise mean curvature on displacements of a coarse solution c and a fine solution f . In Figure 1 we show a pointwise visualization of the difference of curvature between the level 0 and level 3 displacements obtained by respectively SC and PCS on the cloth drape simulation example illustrated in Figure 4 in the main paper. We can similarly measure an alternate distance via the total integral of squared difference in Gaussian curvature, d_K , by replacing H with K .

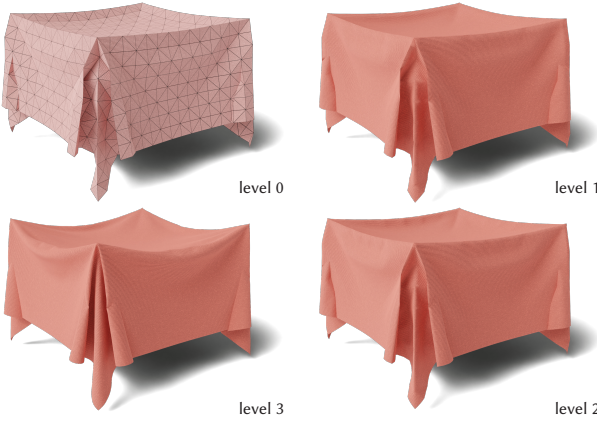


Fig. 3. Artifacts in Sensitive Couture. Creasing and buckling artifacts across resolutions are also generated by Sensitive Couture’s cascadic method in examples, like this pinned drape, without contact and strain-limiting.

In practice, c and f are meshes. The coarse mesh is subdivided until it has the same connectivity as the fine mesh. Curvatures are approximated per-vertex (see below) and then the difference of these vertex quantities integrated according to the parametric domain’s inner product space (mass matrix).

Our preferred metric for cloth simulation is to compare mean curvatures as approximated by quadric fitting [Panozzo et al. 2010], d_H^{fit} . The same approximated curvatures can be used to compare Gaussian curvatures, d_K^{fit} . For completeness and as an emphasis of robustness of this experiment, we compute discrete differential geometry curvatures: d_H^{ddg} using dihedral angles around a vertex [Knöppel et al. 2013] and d_K^{ddg} using angle defect [Meyer et al. 2002].

In Table 1, we compute these quantities for examples in our main text (Fig. numbers cross-referenced). For each model, we compare one or more pairs of levels: “0 → 2” indicates that the coarse level is 0 and the fine level is 2. We compare our method (PCS) to direct Newton solutions and SC [Umetani et al. 2011]. Bold indicates the lower score for each head-to-head comparison (spoiler: it’s always PCS across all measures).

We also include an additional visual comparison via thresholded principal curvature to demonstrate wrinkle consistency across levels of our PCS results (See Figure 2).

2 SENSITIVE COUTURE’S CREASING AND BUCKLING ARTIFACTS

SC artifacts also regularly and easily occur without any contact modeling at all. As a simple demonstration, in Figure 3, we apply a four-level SC model to simulate the drape of a square of cloth, with four pinned points, modeled with default cotton material parameters (no strain-limiting) and with all contact processing disabled. Here, as resolution levels increase from 1K to 64K we continue to see that finer-scale solutions consistently inherit the sharp creasing and buckling artifacts from the coarse solutions all the way to convergence of its finest level.

Table 1. In this table, we report detailed statistics comparing various integrated curvature difference measures. The upshot is that across all experiments and all measures, our PCS method outperforms the competitor (i.e., Newton or SC).

Method	$C \rightarrow F$	$d_H^{\text{fit}} \downarrow$	$d_H^{\text{ddg}} \downarrow$	$d_K^{\text{ddg}} \downarrow$	$d_K^{\text{fit}} \downarrow$
Last column of Figure 16					
PCS	$0 \rightarrow 3$	3.63e+03	1.58e+03	1.16e+07	5.38e+06
Newton	$0 \rightarrow 3$	1.35e+04	2.94e+04	1.20e+08	2.28e+07
Last column of Figure 2					
PCS	$0 \rightarrow 3$	5.63e+03	4.37e+03	1.34e+07	5.89e+06
Newton	$0 \rightarrow 3$	4.91e+05	9.12e+04	8.36e+08	5.04e+09
Armadillo in Figure 12					
PCS	$0 \rightarrow 3$	2.63e+02	2.65e+02	8.14e+05	6.28e+04
Newton	$0 \rightarrow 3$	1.74e+03	1.53e+03	5.84e+06	2.21e+06
Bunny in Figure 12					
PCS	$0 \rightarrow 3$	8.90e+02	8.31e+02	6.00e+06	4.07e+05
Newton	$0 \rightarrow 3$	2.94e+04	2.46e+04	1.10e+08	4.28e+07
Drape over Sphere in Figure 6					
PCS	$0 \rightarrow 1$	1.05e+02	1.39e+02	7.16e+04	2.54e+04
SC	$0 \rightarrow 1$	1.40e+03	4.23e+02	8.25e+05	9.14e+05
PCS	$0 \rightarrow 2$	3.63e+02	3.23e+02	1.81e+05	1.12e+05
SC	$0 \rightarrow 2$	1.56e+04	3.35e+03	2.48e+07	2.76e+07
PCS	$0 \rightarrow 3$	4.03e+02	3.80e+02	7.21e+05	1.33e+05
SC	$0 \rightarrow 3$	2.05e+04	1.75e+04	4.26e+08	1.64e+08
PCS	$1 \rightarrow 2$	1.46e+02	1.28e+02	9.16e+04	7.92e+04
SC	$1 \rightarrow 2$	5.08e+03	5.13e+02	1.33e+06	2.37e+06
PCS	$1 \rightarrow 3$	2.00e+02	1.86e+02	3.41e+05	9.18e+04
SC	$1 \rightarrow 3$	5.30e+03	2.14e+03	2.82e+07	5.86e+07
PCS	$2 \rightarrow 3$	2.40e+01	2.39e+01	9.94e+04	4.00e+04
SC	$2 \rightarrow 3$	7.37e+01	7.77e+01	6.50e+05	5.08e+05

3 CONVERGENCE BEHAVIORS

In Figure 4 we compare a direct Newton solve with globalization (minimizing total energy) to compute convergence of a coarse model’s draping equilibrium, with PCS’s progressive solve to reach the same. We do this for two draping examples. As a baseline for this comparison we also include a direct, coarse quasistatic stepping to reach the same equilibrium. See Table 2 for material and simulation settings. To determine convergence we again apply the same C-IPC [Li et al. 2021] residual of the scaled L^2 norm of the Newton decrement – here using $\epsilon_d = 10^{-3} \text{ m/s}$ (see Section 6.2, “Quality” in the paper) for all three methods. Here we observe, consistent with our results in Section 6.2, “Overhead and Comparative Convergence”, that the number of iterates for direct quasistatic stepping, PCS quasistatic stepping and the Newton solve to directly compute equilibrium all remain close with respective ordering varying per example.

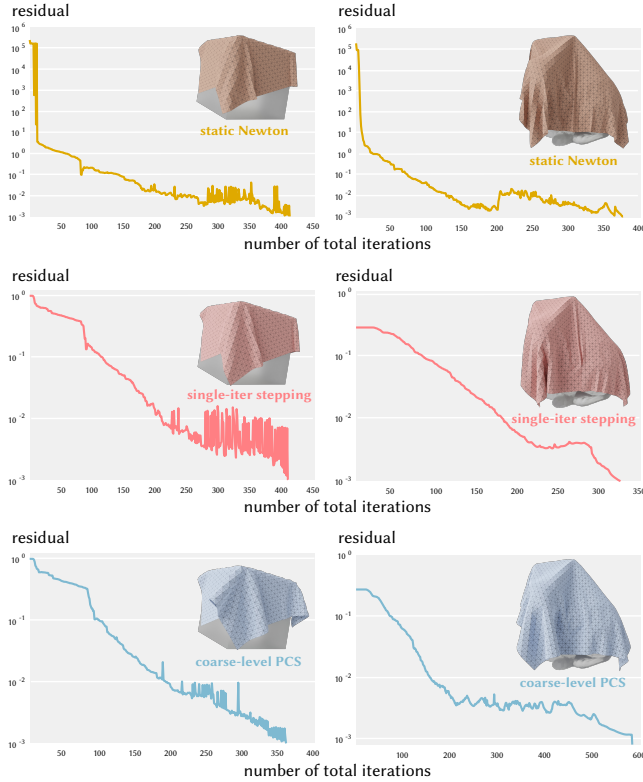


Fig. 4. Convergence comparison between direct static Newton solve (minimizing total energy) to compute convergence (Top), coarse model dрапing equilibrium with single-iteration coarse quasistatic stepping (Middle), and coarse-level PCS (Bottom) to reach the same for drape on square (Left) and bunny (Right) examples. Despite solving an enriched model, PCS convergence remains similar to that of directly solving the unmodified coarse model.

4 TIME-VARYING CONDITIONS

For exploration we drive changes in PCS’s quasistatic simulation over times $t, t + 1, \dots$ by variations (encoded in time-varying u) in material properties, boundary conditions (both Dirichlet and collision geometries), external forces, and handles.

Hard Positional Constraints. When applied, Dirichlet boundary conditions (BC) specify a subset of positionally constrained vertices $\mathcal{B} \subset [1, n]$. For every vertex $x_k, k \in \mathcal{B}$, we have a corresponding target position \tilde{x}_k . In the first Newton iterate of each of each step’s solve, we then start by checking the full step taking all bound vertices in \mathcal{B} to their prescribed targets. We find via step-size filtering a largest possible feasible size step towards these targets and conservatively apply it to update all bound vertices. We then add simple, adaptive quadratic penalties to the objective

$$P(x_k, t) = \frac{\kappa_B}{2} m_k \|x_k - \tilde{x}_k^{t+1}\|^2, \quad (1)$$

where m_k is vertex k ’s lumped mass. We adaptively increase κ_B by $2\times$ whenever the current Newton iterate is close to convergence (via norm of gradient measure) and current targets are not satisfied.

Alternately, if the current iterate satisfies the time step’s targets, we simply fix the bound vertices to their target positions, discard P from the objective and continue Newton iteration to convergence.

Soft Positional Constraints. We enable exploration of physical arrangement and placement over the sequence of time-stepped deformations. To do so we soft-bind handles to BC (unlike the hard BC) above, which allows scripted and interactive exploration of time-varying BC. Here, the application applies a sequence or online stream of per-time step target locations \tilde{x}_k^{t+1} . Our process for resolving them per time step remains otherwise unchanged from our BC treatment above *except* that, rather than adapting, we keep the penalty stiffness κ_B fixed to the bound material’s Young’s modulus.

Collision Geometries. With reliable, always non-intersecting contact processing, cloth model interaction with time-varying collision geometries provides an intuitive and effective means of manipulating cloth drape. Collision geometries—meshes with fully prescribed vertex motion per step—utilize the same BC penalty energy, P as above (from (1)) when moving, while similarly fixing their locations with hard positional constraints when not, without need of membrane and bending energies.

Nested Cages. While collision geometries can be treated (as described above) directly as all other domains in PCS, we alternately can employ Nested Cages [Sacht et al. 2015; Sellán et al. 2021] that are refined in tandem with our primary simulation mesh. Here the nesting property allow us to safely swap in each new refined nested collision geometry from the last while preserving safe initialization; see Figure 9 in our main paper.

Material. For many explorations in design, and modeling the ability to explore changes real-world cloth materials is critical. As discussed in the main, for coarsened simulation this is especially challenging due to the numerical stiffening artifacts introduced by locking errors. We enable direct, smooth changes per step over variations of cloth material moduli (both Young’s and Poisson) in our membrane and bending energies, material thickness (providing direct change in bending stiffness), density, and frictional coefficients in our contact model for varying surface-to-surface stick and slip behaviors.

External and Body Forces. External and body forces such as gravity and inflation are then easily added as user or application-controlled linear potentials.

5 EXAMPLE STATISTICS

In Table 2, we list parameters and model statistics for the PCS examples in our paper. We list resolutions of the coarsest ($\#V_c$) and finest ($\#V_f$) models, the number of refinement levels (#levels), whether strain limiting is in effect (SL), the friction coefficient (μ), the material thickness (d), density (ρ), membrane stiffness (E_{mem}), bending stiffness E_{bend} , and Poisson’s ratio (ν).

REFERENCES

- Felix Knöppel, Keenan Crane, Ulrich Pinkall, and Peter Schröder. 2013. Globally optimal direction fields. *ACM Trans. Graph.* (2013).
 Minchen Li, Danny M. Kaufman, and Chenfanfu Jiang. 2021. Codimensional Incremental Potential Contact. *ACM Trans. Graph.* 40, 4, Article 170 (jul 2021), 24 pages.

Table 2. Model statistics.

Model	# V_c	# V_f	#levels	SL	μ	d	ρ	E_{mem}	E_{bend}	ν
Fig 2 cloth on sphere	3.6K	230K	4	on	0.1	3.18E-04	472.6	8.21E+03	8.21E+03	0.243
Fig 4 cloth on sphere	1.6K	26K	3	off	0.3	3.18E-04	472.6	1.00E+05	1.00E+05	0.3
Fig 4 cloth on cube	1.6K	102K	4	off	0	5.00E-04	472.6	3.00E+05	3.00E+05	0.3
Fig 6 cloth on sphere	1.6K	102K	4	on	0.1	3.18E-04	472.6	8.00E+04	8.00E+05	0.243
Fig 12 Armadillo	2.5K	160K	4	on	0.1	5.64E-04	1000	9.00E+04	9.00E+04	0.349
Fig 12 Bunny	3.0K	194K	4	on	0.4	3.18E-04	472.6	8.21E+03	8.21E+04	0.243
Fig 14 Gorilla	2.5K	160K	4	on	0.1	3.18E-04	472.6	8.21E+03	8.21E+04	0.243
Fig 15 cloth on cube	1.6K	102K	4	on	0.1	3.28E-04	472.6	7.60E+02	7.60E+03	0.071
Fig 11 - column 1	1.6K	102K	4	on	0.1	3.18E-04	472.6	8.21E+03	8.21E+04	0.243
Fig 11 - column 2	1.6K	102K	4	on	0.1	3.18E-04	472.6	8.21E+03	8.21E+04	0.243
Fig 11 - column 3	1.6K	102K	4	on	0.1	3.18E-04	472.6	8.21E+03	8.21E+04	0.243
Fig 13 cloth on dragon	1.5K	370K	5	on	0.1	3.18E-04	472.6	8.21E+03	8.21E+04	0.243
Fig 16 - column 1	1.6K	102K	4	off	0.1	3.18E-04	472.6	8.21E+05	8.21E+05	0.243
Fig 16 - column 2	1.6K	102K	4	on	0.1	3.18E-04	472.6	8.21E+03	8.21E+04	0.243
Fig 16 - column 3	3.6K	230K	4	on	0.1	3.18E-04	472.6	8.21E+03	8.21E+03	0.243
Fig 16 - column 4	1.6K	102K	4	on	0.1	1.80E-04	83	5.70E+03	5.70E+04	0.3
Fig 16 - column 5	1.6K	102K	4	on	0.1	6.60E-04	400	2.50E+04	2.50E+05	0.361
Fig 16 - column 6	1.6K	102K	4	on	0.1	3.28E-04	543	7.60E+02	7.60E+03	0.071
Fig 8 ribbon	0.1K	48K	5	off	0	6.724E-04	596.3	5.709E+05	5.709E+05	0.421
Fig 7 - tablecloth	1.5K	93K	4	off	0.4	2.664E-04	601.1	9.036E+04	9.036E+04	0.349
Fig 7 - handkerchief	0.2K	14K	4	off	0.4	1.187E-03	193.7	3.158E+04	3.158E+04	0.25
Fig 2 - supplemental	2.5K	160K	4	on	0.1	5.64E-04	1000	9.00E+04	9.00E+04	0.349
Fig 3 - supplemental	1.0K	64K	4	off	0	3.18E-04	500	3.00E+05	3.00E+05	0.3

Mark Meyer, Mathieu Desbrun, Peter Schröder, and Alan H. Barr. 2002. Discrete Differential-Geometry Operators for Triangulated 2-Manifolds. In *VisMath*, Hans-Christian Hege and Konrad Polthier (Eds.).
Daniele Panozzo, Enrico Puppo, and Luigi Rocca. 2010. Efficient Multi-scale Curvature and Crease Estimation. *GraVisMa* (2010).
Leonardo Sacht, Etienne Vouga, and Alec Jacobson. 2015. Nested Cages. *ACM Transactions on Graphics (TOG)* 34, 6 (2015), 1–14.

Silvia Sellán, Jack Luong, Letícia Mattos Da Silva, Aravind Ramakrishnan, Yuchuan Yang, and Alec Jacobson. 2021. Breaking Good: Fracture Modes for Realtime Destruction. *arXiv preprint arXiv:2111.05249* (2021).
Nobuyuki Umetani, Danny M. Kaufman, Takeo Igarashi, and Eitan Grinspun. 2011. Sensitive Couture for Interactive Garment Modeling and Editing. *ACM Trans. Graph.* 30, 4, Article 90 (jul 2011), 12 pages.